

# New Physical Model for Lifetime Estimation of Power Modules

I. F. Kovačević, U. Drofenik, and J. W. Kolar

ETH Zurich, Power Electronic Systems Laboratory, Physikstrasse 3, 8092 Zurich, Switzerland  
kovacevic@lem.ee.ethz.ch

**Abstract**—In this paper a physical model for lifetime estimation of standard power modules is proposed. The lifetime prediction is based on the assumption that the solder interconnections are the weakest part of the module assembly and that the failure cause is the inelastic deformation energy accumulated within the solder material. Unlike the well-known Coffin-Manson model, the proposed model can be used to physically explain the dependency of lifetime on the various properties of a temperature profile i.e. frequency, dwell-ramp time, minimum/maximum temperature. The model is based on Clech's algorithm for simulation of stress-strain solder response under cyclical thermal loading and on the solder deformation mechanism map used to define the dominant failure mechanism under observed stress-temperature conditions. Either accelerated cycling tests or existing field databases are needed to parameterize the model. To verify the approach, the results of power cycling tests for a high power IGBT module found in literature are applied and the impacts of two mission profiles on the module lifetime are examined.

**Index Terms**—Clech's algorithm, deformation mechanism map, lifetime modeling, mission profile.

## I. INTRODUCTION

Specifying, designing and maintaining power electronics systems is a complex task since there is an ever increasing demand for higher reliable products in all industries. Reliability is an important issue for power electronics systems that require long-term lifetime guarantees like those used in cars, locomotives, airplanes etc. Power electronics converter employed in these systems are exposed to rather severe operating conditions: high voltages and currents, temperature cycles of large amplitude, etc., and the reliability of a whole system is determined by the endurance of each element i.e. each power module comprising high power IGBTs or MOSFETs and diodes.

A standard power module can be seen as a multilayered structure (see Fig. 1). The heat dissipated inside a power semiconductor chip is conducted through the multilayered structure into a heat sink, and it is then transferred by convection through the heat sink to the ambient. Due to their low cost and appropriate physical properties high power modules with lead-based solder interconnections (eutectic SnPb, or high lead solders PbSn with a small addition of silver) are still in use. However, since lead adversely impacts the environment and health, other candidates like SnAg alloys attract more attention nowadays.

The layers, having typically different thermal properties, have great influence on the heating and cooling rates of the module and determine its overall performance. Consequently, the failures of power modules are directly related to the power modules' assembly structure and packaging technology. During thermal and/or termo-mechanical loadings, the module assembly layers experience shear stresses due to the differing coefficients of thermal expansion (CTE), i.e. the bimetallic effect. The failure modes observed so far in modern power modules are described in [1].

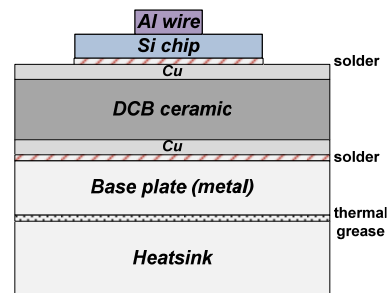


Fig. 1. Multilayered structure of a standard power module: power semiconductor chips are soldered to a direct bonded copper (DBC) ceramic substrate [2]; at the bottom side, the substrate is soldered to the package (metal) base plate; the chip interconnections are performed by aluminium (Al) wire bonds; the layer thickness are not shown to scale.

To study dominant wear-out failure mechanisms of power modules, active power and passive temperature cycling tests are performed. Setting test conditions to induce a specific failure mechanism is the most important issue in such accelerated experiments. So far, the known weak points are the interconnections inside the power module including wire bonds and solder joints i.e. die attachment and the joint between the base plate and the substrate. The most common failures occurring at these interconnections are mainly ascribed to unmatched coefficients of thermal expansion (CTE) of adjacent materials: wire bond and silicon, silicon and DBC substrate, DBC substrate and base plate.

In recent years advanced wire bonding techniques have been applied suggesting that the bond wire lift-off failure mode might be avoided with certainty [3]. Furthermore, effort has been made to analyze solder layers in more detail i.e. to develop an accurate lifetime model for solder joint failures. So far, extensive research has been done to develop an accurate lifetime prediction for power modules but a generally applicable model is still not developed.

## II. POWER MODULE LIFETIME PREDICTION

Several well-known lifetime models are summarized in this section to gain a brief insight into the current state of research in the field. In general, two different lifetime modelling approaches can be distinguished: analytical and physical. The models are built based on the thermo-mechanical characteristics of the module assembly, on the knowledge of failure mechanisms under certain conditions, and on the mission profile dedicated to the module i.e. the temperature profile  $T(t)$  appearing within the solder layer of a module during its operation.

### A. Analytical Lifetime Models

Analytical models describe the dependence of the number of cycles to failure ( $N_f$ ) on the parameters of temperature cycles i.e. amplitude, duration, frequency, mean value, dwell time, maximum and minimum temperature, etc. Several analytical models published in literature are analysed: the Coffin-Manson model [4], Norris-Landzberg model [5], and Bayerer's model [6].

The well-known Coffin-Manson model has been widely used even though it has obvious shortcomings.

$$N_f = a \cdot (\Delta T_j)^{-n} \cdot e^{E_a/(k \cdot T_m)} \quad (1)$$

According to the Coffin-Manson formula (1), the number of cycles to failure depends only on the temperature amplitude of the junction temperature  $\Delta T_j$  and the medium temperature  $T_m$ . As it has been proven [6, 7] that the other parameters i.e. frequency of cycles, heating and cooling times also take significant influence on lifetime, the Coffin-Manson model is rather simple and not accurate enough.

The second considered analytical model is the Norris-Landzberg model, which includes the frequency parameter but neglects the influence of other parameters such as heating and cooling time,

$$N_f = A \cdot f^{-n_2} (\Delta T_j)^{-n_1} \cdot e^{E_a/(k \cdot T_{\max})} \quad (2)$$

The multi-parameter model of Bayerer (3) is the most comprehensive analytical model as it is built based on a large amount of power cycling data from different module technologies. It includes the influence of the various parameters of power cycling tests and also power module characteristics: temperature swing  $\Delta T_j$ , the maximum junction temperature  $T_j$ , the heating time  $t_{on}$ , the applied DC current  $I$ , the diameter  $D$  of the bond wires and the blocking voltage  $V$ .

$$N_f = K (\Delta T_j)^{\beta_1} \cdot e^{\beta_2/(T_j+273K)} \cdot t_{on}^{\beta_3} \cdot I^{\beta_4} \cdot V^{\beta_5} \cdot D^{\beta_6} \quad (3)$$

The constants  $K$  and  $\beta$  are extracted from a large data set collected in the long-term reliability testing experiments.

Assuming that the failure of solder interconnections is the dominant failure mechanism, a more accurate approach would be to use the solder layer temperature [8] in these  $N_f$ -models instead of the junction temperature  $T_j$  measured on the top of chip.

Lifetime prediction of a power module using an analytical approach is performed by means of Miner's rule for damage accumulation. The correlation between temperature changes and the damage produced within the module has to be defined and then lifetime is represented as inverse of the total damage accumulated within a power module until the cessation of its correct functioning. In a real operating environment power modules are exposed to rather non-uniform temperature variations and thus for the analytical lifetime modelling a proper definition of a temperature cycle within the given mission profile is required. Accordingly, mission-profile-transformation into a sequence of temperature cycles is the main issue of the analytical approach.

The performance of three observed analytical models can be analyzed using the results of the power cycling tests ( $N_f$  results) for high power IGBT traction modules (Table I) [7]. Table I summarizes  $N_f$  results for three power cycling tests PC<sub>1-3</sub> with equal temperature swings but different heating and cooling times. The number of cycles to failure predicted by the analytical models and the experimental  $N_f$  results in Table I are compared by (4) and (5).

Apparently, the results in Table I cannot be explained by the Coffin-Manson model. On the other hand, if the power cycling tests PC<sub>1</sub> and PC<sub>2</sub> are employed to find the unknown parameter  $n_2$  in the Norris-Landzberg equation and the  $N_f$  for PC<sub>3</sub> is calculated by (2), then the resulted  $N_f$  would be 2.1 times higher than the experimentally reported value in Table I. This implies that (2) underestimates the lifetime of the observed IGBT modules. Similarly, using (3)  $N_f$  ratios can be calculated and then compared to the experimental ratios defined by Table I. The resulting  $N_f$  ratios are given by (4) and (5),

$$\frac{N_{f,PC_1}}{N_{f,PC_2} \text{ (3)}} = 1.54, \quad \frac{N_{f,PC_1}}{N_{f,PC_3} \text{ (3)}} = 2.36 \quad (4)$$

$$\frac{N_{f,PC_1}}{N_{f,PC_2} \text{ (Table I)}} = 2.77, \quad \frac{N_{f,PC_1}}{N_{f,PC_3} \text{ (Table I)}} = 11.91. \quad (5)$$

The difference between (4) and (5) points out that Bayerer's model does not comply with the experimental results presented in Table I.

TABLE I  
POWER CYCLING TESTS FOR THREE POWER TRACTION MODULES

Module	$\Delta T_j$ [°C]	$T_{j,max}$ [°C]	$I_C$ [A]	$t_{on}$ [s]	$t_{off}$ [s]	$N_f$ [-1k]
PC1	50	110	166	3.1	2.3	305
PC2	50	110	149	10	4	110
PC3	50	110	138	30	4.6	25.6

### B. Physical Lifetime Models

Physical modelling requires failure and deformation mechanisms to be priorly known. It is based on the knowledge of stress/strain deformations within devices that can be gained either by experiments or simulations. Direct measurements of stress and strain in electronic packages demand the usage of high resolution measuring

methods i.e. infrared microscopy, etc. Therefore, computational mechanics, like Finite Element Analysis (FEA), are often employed.

The physical models for estimating the lifetime of Al bond wires are based on fracture mechanics and basically rely on FE simulations ([9]). On the other hand, physical models of solder behaviour under thermal cycling operation have been developed for high-density electronics packages mostly used in telecommunication and consumer electronics: flip chips, ball grid arrays (BGA), chip size packages (CSP), and fine-pitch surface mounted assemblies. These models are essentially based on the experimental data collected in low-cycle tests needed for model parameterization. Hence, the corresponding databases for frequently employed solder materials can be found in literature.

Four classes for the lifetime prediction of solder joints can be distinguished: stress-based methods, strain-based methods, energy-based methods, and damage-based methods. Energy-based models are seen to be the most convenient, as they have ability to capture test conditions with more accuracy [10].

An energy-based method specially intended for power modules is introduced in [11]. The stress-strain response to an arbitrary temperature profile of a bimetallic interconnection is numerically calculated and the resulting stress-strain curve is further used to calculate the total deformation energy accumulated within the module. The lifetime model presented in [11] is based on the assumption that the end-of-life of a device is determined by the total deformation energy accumulated during the operation of a device: a device fails when the deformation work reaches the critical value  $\Delta W_{tot}$ . The main drawback of this model is that elastic and plastic deformations are neglected in the stress-strain relation formulas and only time-dependent creep is taken into account.

A new physical model for lifetime estimation of power modules relying fundamentally on the energy-based approach is proposed in the next section. The physical model enables lifetime estimation of power modules which should operate under arbitrary temperature profiles.

### III. THE PROPOSED PHYSICAL LIFETIME MODEL

The proposed method for lifetime estimation of power modules is derived from comprehensive equations describing solder behaviour, i.e. simultaneously taking into account elastic, plastic and creep deformation. The stress-strain curves are obtained from modelling solder response to different temperature profiles. Then, applying the energy-based approach, these equations are used to calculate the total deformation energy producing the final device failure. The stress-strain response of a solder joint is generated by means of Clech's algorithm [12]. The brief summary of the theory behind the proposed model is given in the following subsections.

#### A. Solder Behavior

Solder response to a thermal cycling load can be

described by means of a hysteresis loop. As a result, the stress-strain plot can be employed as a tool for lifetime estimation of solder joints in electronic devices. Depending on the stress level and temperature, solder experiences different physical deformations that gradually contribute to damage accumulation and finally to the failure of solder interconnections. The stress-strain response is modelled by solder constitutive equations that mathematically describe time-independent elastic and plastic deformations and time-dependent plasticity called creep.

By their nature, elastic and plastic deformations and creep can be defined respectively by strain and strain-rate functions,

$$\begin{aligned} \gamma &= f(\tau, T) \\ d\gamma / dt &= f(\tau, T, t) \end{aligned} \quad (6)$$

where  $\gamma$  is strain,  $\tau$  is stress,  $T$  is the temperature and  $t$  is time. According to mechanical analysis [13], the connection between shear stress and strain within a solder joint can be described by the reduction lines (7), where  $K$  is the reference assembly stiffness depending on geometry (the height  $h$  and the cross section of solder joint  $A$ ) and  $D_1$  is a constant reflecting both the geometry (the length of solder joint  $L$ ) and CTE mismatch between layers connected by solder,  $\alpha_1 - \alpha_2$ . The explanation of reduction lines is given in Fig. 2.

$$\begin{aligned} \gamma_{shear} + \frac{\tau_{shear}}{K} &= D_1 \cdot (T - T_0) \\ K &\sim \frac{h}{A}, \quad D_1 = L \cdot (\alpha_1 - \alpha_2) \end{aligned} \quad (7)$$

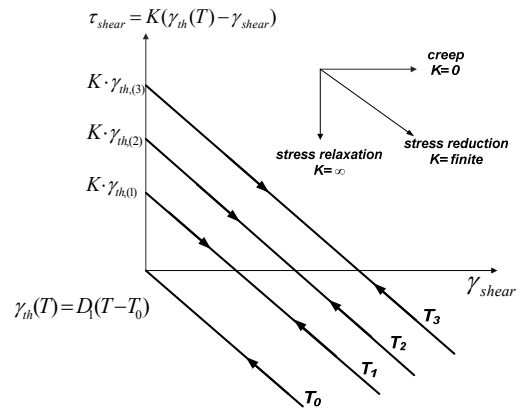


Fig. 2. Isothermal stress reduction lines at different temperatures and comparison of stress reduction to stress relaxation and creep.

The assembly layers change their dimensions according to their CTEs. The strain created by thermal mismatch of materials joined by solder is accommodated within the solder layer by the strain change  $\Delta\gamma$  composed of a plastic, elastic and/or creep component. The equations describing solder behavior are given by (8)-(11).

Based on Hook's law, elasticity of solder can be defined by

$$\gamma = \frac{\tau}{G(T)}. \quad (8)$$

To describe time-independent plastic behavior Darveaux's stress-strain ( $\tau$ ,  $\gamma$ ) dependency [14]

$$\gamma = C_p \cdot \left(\frac{\tau}{G(T)}\right)^{m_p} \quad (9)$$

is used, where  $G$  is the shear modulus constant dependent on temperature,  $G(T) = G_0 - G_1(T - 273K)$ .

Analyzing the creep nature of solder, two types of creep deformation can be distinguished: dislocation controlled creep at higher and diffusion controlled creep at lower stress levels, defined respectively by strain rate equations (10) and (11).

$$\begin{aligned} \frac{d\gamma}{dt} = & C_l \cdot \frac{G(T)}{T} \sinh\left[\left(\frac{\alpha \cdot \tau}{G(T)}\right)^{n_l}\right] \cdot e^{-Q_l/RT} \\ & + C_h \cdot \frac{G(T)}{T} \sinh\left[\left(\frac{\alpha \cdot \tau}{G(T)}\right)^{n_h}\right] \cdot e^{-Q_h/RT} \end{aligned} \quad (10)$$

$$\begin{aligned} \frac{d\gamma}{dt} = & B_1 \cdot \frac{G(T)}{T} \cdot \left(\frac{\tau}{G}\right) \cdot e^{-Q_b/RT} \\ & + B_2 \cdot \frac{G(T)}{T} \cdot \left(\frac{\tau}{G}\right) \cdot e^{-Q_m/RT} \end{aligned} \quad (11)$$

Each strain rate equation consists of two parts referring to different deformation mechanisms at low and high temperature ranges. To cover the full stress range both creep equations are needed. The term  $G/T$  has been introduced to take into account the temperature effect. The constants and parameters for 63Sn37Pb solder can be found in [15]. It was shown in [15] that these constitutive equations could be used to describe the creep deformation of solder for different temperatures over a wide stress range.

### B. Deformation Mechanism Map

The nature of deformations occurring within metals and ceramics exposed to some external stresses, e.g. thermal stresses, is explained in detail in [16]. The deformation mechanism map is a stress-temperature diagram presenting the dependency of normalized stress  $\tau/G$  on homologous temperature  $T/T_M$  ( $T_M$  is the melting temperature). For a known stress and temperature range, the dominant damage mechanism can be identified from the map. An example of a deformation mechanism map is presented in Fig. 3 with the axis scaled just as a guide.

The regions of the deformation mechanism map are defined by the solder constitutive equations (8)-(11). The borders between low temperature and high temperature creep regions can be found by equalizing the left and the right terms of (10) or (11). In the same manner, the stress-temperature condition for transition from one creep mechanism to another can be calculated by equalizing (10) and (11).

### C. Clech's Algorithm

Clech's intention was to find a way to accurately simulate the response of SMT solder joints exposed to

cyclic load. The resulting algorithm for generating a stress-strain response for eutectic solder is introduced in [12].

Clech's algorithm can be explained by Fig. 3. Knowing the stress-strain state ( $\gamma_1$ ,  $\tau_1$ ) at time  $t$ , the stress-strain state ( $\gamma_2$ ,  $\tau_2$ ) at time  $t + \Delta t$  can be calculated using the constitutive equations describing solder behaviour. It is assumed that: (a)  $\Delta t$  is a relatively small time step, (b) the stress is built up instantaneously for the temperature increase from  $T = T_1$  to  $T_2 = T_1 + \Delta T$ , assuming that dominant strain components are time-independent plastic and elastic components  $\Delta\gamma_{elastic}$  and  $\Delta\gamma_{plastic}$ , and (c) at temperature  $T_2$ , the change of stress follows the  $T_2$ -reduction line building the strain component  $\Delta\gamma_{creep}$ .

To calculate  $\Delta\gamma_{elastic}$  and  $\Delta\gamma_{plastic}$ , (8) and (9) are used and  $\Delta\gamma_{creep}$  is calculated using either (10) or (11). The implemented algorithm detects changing from one region into a neighboring region of the deformation mechanism map and selects the according creep differential equation.

This approach provides the explanation of solder behaviour under different temperature profiles. The influence of ramp time, hold time, and frequency of cycling can be captured by the information carried within the corresponding hysteresis (stress-strain curve) returned by the described simulation.

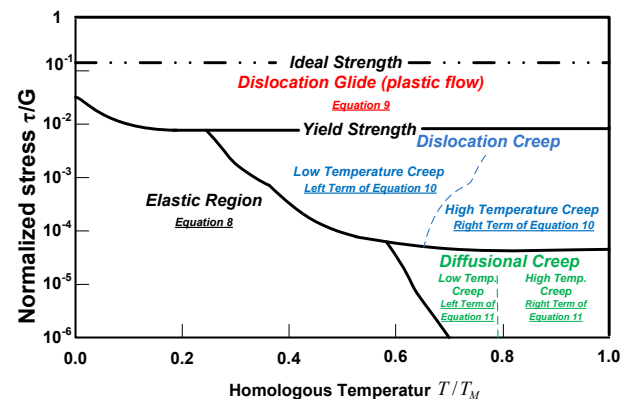


Fig. 3. The regions of the deformation mechanism map are described by corresponding solder constitutive equations.

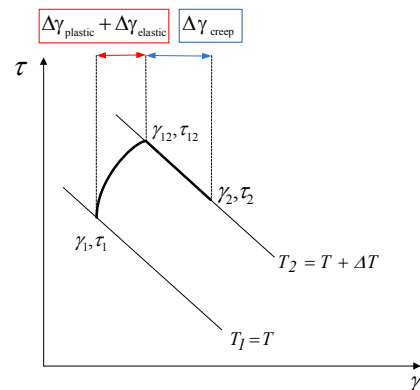


Fig. 4. The solder stress-strain simulation step for a temperature increase from  $T_1$  to  $T_2 = T_1 + \Delta T$ .

Implementing Clech's algorithm based on (8)-(11) in MATLAB allows to numerically solve the solder

constitutive equations and to calculate hysteresis loops corresponding to temperature cycling tests or an input temperature profile (mission profile) with an arbitrary shape.

#### IV. RELATIVE LIFETIME ESTIMATION

In combination with the deformation mechanism map, the constitutive solder equations are used to accurately determine strain components in the entire stress and temperature range. The proposed lifetime model needs 17 material/geometry parameters to be known. The material parameters of 60Sn40Pb (i.e. 63Sn37Pb) solder typically used in standard power modules are taken from [14] and [15].  $K$  and  $D_I$  are material/geometry dependent parameters that have to be additionally determined as described in the following.

##### A. Model Parameterization

To fully parameterize the model, the results of at least two accelerated power cycling tests are needed i.e. the number of cycles to failure for different temperature profiles,  $N_{f1}$  and  $N_{f2}$ . The total deformation energy  $W_{tot,k}$  accumulated in the solder layer that leads to the module's end of life can be calculated by

$$W_{tot,k} = N_{f,k} \cdot W_{hys,k} \quad (7)$$

where  $N_{f,k}$  is the number of cycles to failure for the  $k$ -th temperature profile and  $W_{hys,k}$  is the deformation energy equal to the area of one corresponding simulated hysteresis loop. For power modules of same type,  $W_{tot,k}$  should theoretically be constant. An optimization routine is used to find the best set of parameters ( $K, D_I$ ) so that the ratio,  $W_{tot1}/W_{tot2}$ , is close to one. The power cycling tests have to be specified such that all deformation mechanisms are invoked. The parameterization procedure can be described by the flow chart in Fig. 5.

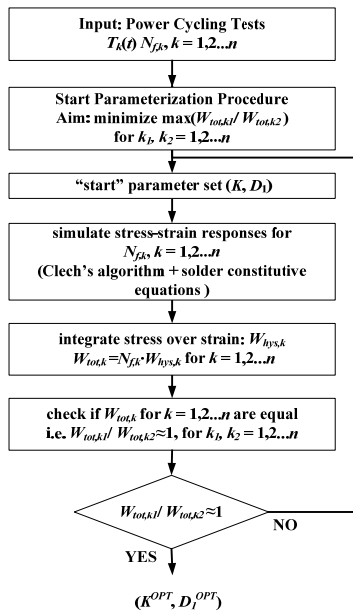


Fig. 5. Flow chart describing the parameterization of the proposed lifetime model.

The parameterization of the proposed physical model is defined as an optimization routine implemented in MATLAB. The optimal parameters should minimize the difference of two calculated deformation energies  $W_{tot,k1}$  and  $W_{tot,k2}$  corresponding to two different input temperature profiles  $T_{k1}$  and  $T_{k2}$ . The ratio of the parameterization defined as (8) should be ideally equal to 1,

$$r = W_{tot,k1} / W_{tot,k2} \quad (8)$$

The search procedure for the optimal unknown parameters is based on a built-in MATLAB optimization routine that returns only local minimums and cannot guarantee finding the global minimum of the objective function. Therefore, an approach to deal with local minimums is needed in order to ensure the choice of the right parameters  $K$  and  $D_I$ . An idea to find out which parameter set most correctly describes theoretical solder behaviour is suggested in Section IV.C.

##### B. Verification of the Proposed Lifetime Modeling Approach

To verify the proposed lifetime prediction approach, the presented physical model is applied to a high power IGBT traction module already discussed in Section II.A. The model parameterization is performed using the results of three power cycling tests (see Table I) with temperature profiles presented in Fig. 6. The power cycling tests were originally performed to identify the influence of cycling time on the lifetime behavior of IGBT modules. Therefore, in all three power cycling tests, the temperature swings were set to 50°C with the maximum temperature of 110°C. The final failure driving force was ascribed to solder interconnections.

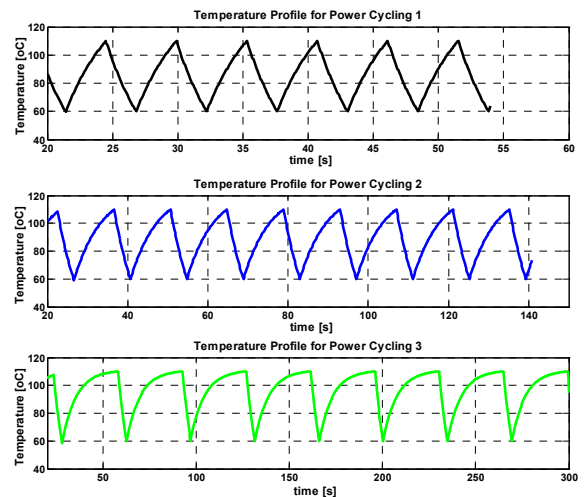


Fig. 6. The temperature profiles during three power cycling tests of the IGBT traction modules defined in Table I.

Following the procedure described by the flow chart in Fig. 5, several optimal parameter sets ( $K, D_I$ ) are found. Two parameter sets,  $s_{1,2} = (K, D_I)$  (see Table II) returning a similar ratio of parameterisation are chosen to analyze the simulation results and to describe an idea how the stress-strain curves for different parameter sets can be distinguished among each other.

TABLE II  
TWO OPTIMAL PARAMETER SETS RETURNED BY THE  
PARAMETERIZATION PROCEDURE

Parameter Set	K	D <sub>1</sub>	Ratio
s <sub>1</sub>	2454	2.7e-4	1.614
s <sub>2</sub>	1034	7.3e-4	1.586

The simulations of solder stress-strain response using s<sub>1</sub> and s<sub>2</sub> are depicted respectively in Fig. 7 and Fig. 8. The y-axis represents stress in MPa, while the x-axis represents strain i.e. strain scaled by the height of the solder joint, in percent. From the figures, it can be seen that the hystereses shapes and the stress levels are similar, but the strain magnitudes belong to different ranges so that the hystereses are shifted from each other along the strain axis.

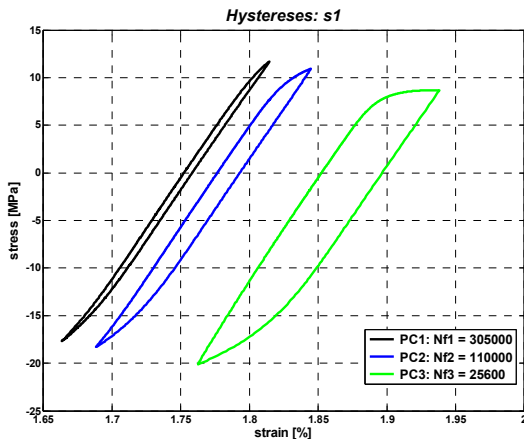


Fig. 7. The stress-strain simulation applying the parameters set s<sub>1</sub> = (K, D<sub>1</sub>) for the IGBT traction modules exposed to three power cycling profiles PC<sub>1-3</sub>.

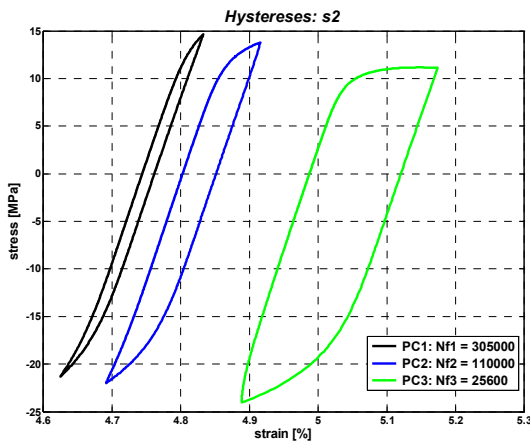


Fig. 8. The stress-strain simulation applying the parameters set s<sub>2</sub> = (K, D<sub>1</sub>) for the IGBT traction modules exposed to three power cycling profiles PC<sub>1-3</sub>.

Regarding the ratio of parameterization, it was observed that better results would be achieved if the failure criterion of IGBT modules was differently chosen i.e. 50% increase of junction thermal resistance R<sub>thj</sub> instead of 20%. The N<sub>f</sub>-results for these two criteria are compared in Table III. Using the experimental N<sub>f</sub>-results returned by the 50% failure criterion as input of the parameterization procedure, the calculated ratio of parameterization is on average 1.1. This implies that the

results of power cycling tests used to parameterize the model have significant influence on the determination of the unknown material/geometry parameters.

TABLE III  
THE POWER CYCLING RESULTS FOR TWO DIFFERENT LEVELS OF FAILURE  
CRITERION: 20% AND 50% INCREASE OF R<sub>thj</sub>

Module	20% increase of R <sub>thj</sub>	50% increase of R <sub>thj</sub>
PC1	305 000	480 000
PC2	110 000	186 000
PC3	25 600	59 400

### C. Selection of Optimal Parameters K and D<sub>1</sub>

The total strain is the sum of the creep and time-independent plastic and elastic strain components. The numerical implementation makes possible to separately evaluate the strain components and to find out which component becomes more dominant in which part of temperature cycle. Analyzing how strain develops during a temperature cycle, gives deeper theoretical insight into the solder behaviour and enables to investigate the influence of the unknown material/geometry parameters on stress-strain response.

Based on theory, creep cannot be developed at fast temperature rates and time-independent plasticity and elasticity produce the most of strain deformations in that case. On the other hand, at lower temperature rates, creep becomes gradually dominant and determines almost alone the total strain. Consequently, for a comprehensive analysis, it is important to choose the temperature profiles such that the impact of both creep and time-independent plastic and elastic deformations can be observed. Accordingly, the creep behavior should be best observed in PC<sub>3</sub> with the longest turn-on time, while for PC<sub>1</sub> with fast temperature changes the time-independent plastic and elastic components should be dominant over the creep strain component. The strain components for the temperature profiles PC<sub>1</sub> and PC<sub>3</sub> are presented respectively in Appendix Fig. A2 and Fig. A3.

For the parameter set s<sub>1</sub>, plasticity and elasticity almost solely determine the total strain during the whole temperature cycle PC<sub>1</sub> (Fig. A2a), but in the simulation with the parameter set s<sub>2</sub> the creep component takes some higher share in the total strain at the end of both down- and up-ramp times of the temperature cycle PC<sub>1</sub> (Fig. A2b).

In the case of temperature profile PC<sub>3</sub> with slower temperature changes, it can be seen that the creep component becomes dominant at the dwell period of temperature cycle (Fig. A3), building almost solely the total strain in both simulations with s<sub>1</sub> and s<sub>2</sub>. These results comply with theoretical behaviour of solder material. However, an apparent difference between the simulations with the parameter sets s<sub>1</sub> and s<sub>2</sub>, is the magnitude of creep component at the up- and down-ramp times of PC<sub>3</sub> i.e. for faster changes of PC<sub>3</sub>. In the simulation with s<sub>1</sub>, the creep is always smaller than the time-independent plasticity, while in the simulation with s<sub>2</sub>, the value of creep component becomes almost equal to the value of time-independent strain.

Accordingly, it can be concluded that by taking the parameters set  $s_2$  as input for the simulation, the creep component is higher for both temperature profiles  $PC_1$  and  $PC_3$  so that the stress-strain simulation with the parameter set  $s_1$  better agrees with the theory of solder behaviour.

#### D. Lifetime Prediction Approach

Having parameterized the solder model, different mission profiles can be compared to estimate the worst operation conditions of the power module. For two mission profiles,  $T_1(t)$  and  $T_2(t)$  the stress-strain simulation returns two hystereses carrying the information about the solder deformation losses ( $W_{tot1}$ , and  $W_{tot2}$ ). Equation (8) defines the relative lifetime of the power module.

$$r = \frac{W_{tot1}}{W_{tot2}} = \frac{\int_{T_1(t)} \tau d\gamma}{\int_{T_2(t)} \tau d\gamma} \quad (8)$$

The ratio (8) means that the first profile results in  $r$  times more deformation damage than the second profile implying that an increase of the lifetime of semiconductors by a factor  $r$  can be expected if  $T_2(t)$  is applied instead of  $T_1(t)$ . The lifetime prediction can be demonstrated on an example of two mission profiles A and M from [17]. The resulting stress-strain simulations applying the parameter set  $s_1$  are presented in Fig. 9 and 10. The relative lifetime is found to be  $r = 2.5$  (9).

$$r = \frac{W_{totA}}{W_{totM}} = 2.5 \quad (9)$$

It means that the small oscillations of temperature within the temperature profile A would produce more damage to an IGBT traction module than would be produced by the constant temperature levels within the mission profile M.

#### V. CONCLUSIONS

The proposed physical model for lifetime prediction of power modules is developed based on Clech's algorithm and the energy-based lifetime modelling approach. The used solder constitutive equations simultaneously take into account different deformation mechanisms: elasticity, plasticity and creep. The implemented numerical simulation returns the hysteresis-loops of the stress-strain behaviour taking as input an arbitrary temperature profile  $T(t)$ . The model has the ability to handle all information comprised within the mission profile.

The transformation of a mission profile into the frequency distribution of temperature changes, characteristic to analytical methods, is avoided. This increases the accuracy of the proposed approach significantly, but still power cycling test results are needed to accurately parameterize the model. Typically, power electronic engineers do not know the full internal physical structure of power modules which would be required in FE analysis and also they are not specialized in characterizing materials what is a much closer topic to

mechanical engineering. Therefore, the approach proposed in this paper enables engineers to estimate the lifetime of power modules without detailed specifications and without the knowledge of geometric properties which are hard to measure. At the same time, it is less demanding than FE analyses from the aspects of computational complexity and run-time.

The verification of the model is demonstrated on the example of a power cycling test taken from literature [7]. The parameterization procedure is described through a flow chart diagram and the simulated stress-strain curves for two different parameter sets producing similar error of parameterization are analyzed. In a next step at the PES Laboratory of ETH Zurich, power cycling equipment will be built which allows to define temperature cycles of arbitrary shape in order to further evaluated the proposed physical model [18].

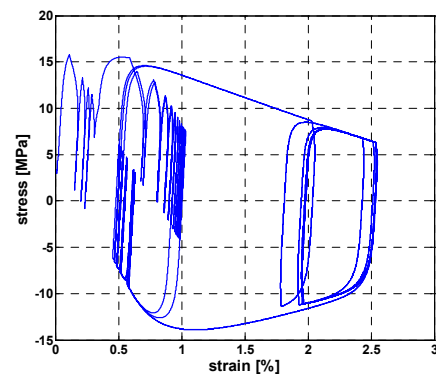


Fig. 9. Stress-strain response to the temperature profile A of [16].

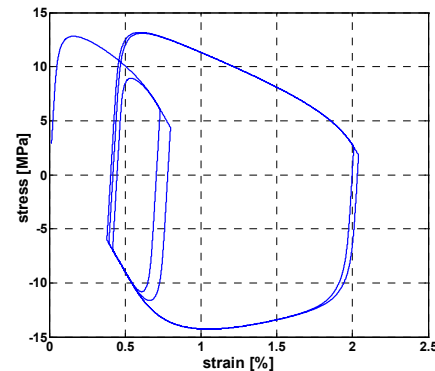


Fig. 10. Stress-strain response to the temperature profile M of [16].

#### APPENDIX

The stress and strain variations for third temperature cycling profile are separately shown in Fig. A1. It can be seen that stress is proportional to temperature and strain changes nonlinearly with temperature. The temperature profiles and the corresponding strain components, split into the time independent plastic/elastic  $\Delta\gamma_{pl\&el}$  (blue) and time-dependent creep parts  $\Delta\gamma_{creep}$  (green), are shown in Fig. A2 and Fig. A3. The fast slopes of strain components actually correspond to the derivative of strain as the constant time step is used in the simulation,  $\Delta\gamma = \Delta t \cdot d\gamma/dt$ .

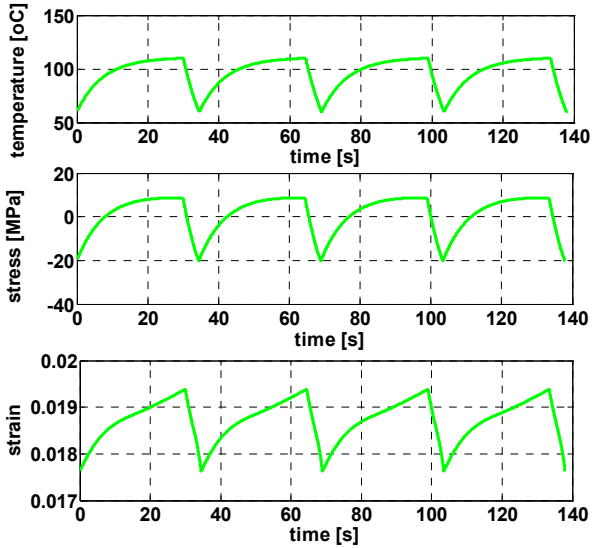


Fig. A1. Strain and stress variations for the temperature profile PC<sub>3</sub> applying the parameters set s<sub>1</sub>.

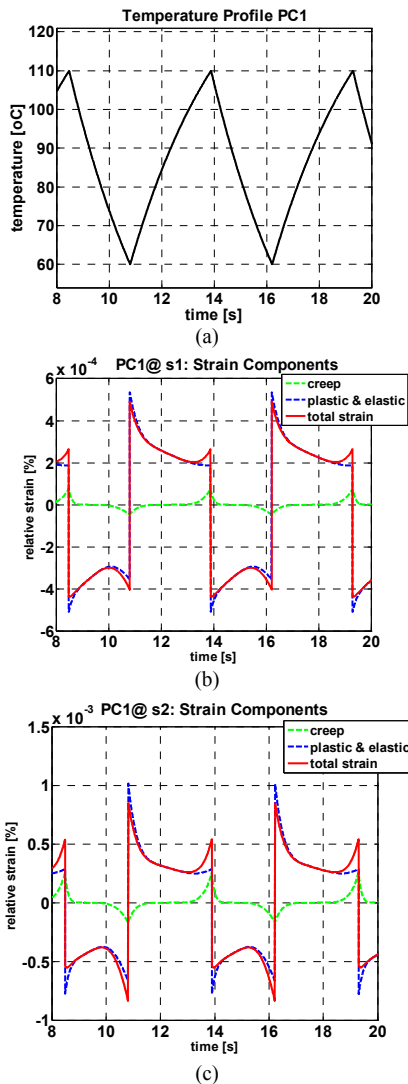


Fig. A2. Analysis of strain components: (a) temperature profile PC<sub>1</sub>, (b) strain components applying the parameters set s<sub>1</sub>, (c) strain components applying the parameters set s<sub>2</sub>.

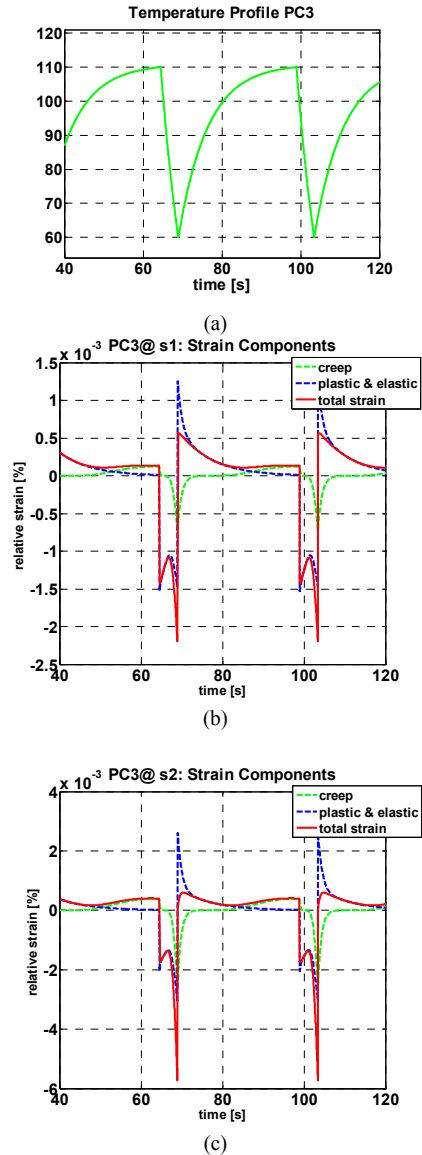


Fig. A3. Analyses of strain components: (a) temperature profile PC<sub>3</sub>, (b) strain components applying the parameters set s<sub>1</sub>, (c) strain components applying the parameters set s<sub>2</sub>.

REFERENCES

- [1] M. Ciappa, "Selected failure mechanisms of modern power modules", *Microelectronics Reliability*, vol. 42, no. 4, pp. 653-667(15), April 2002.
- [2] U. Drofenik, D. Cottet, A. Müsing, J. M. Meyer, and J. W. Kolar, "Modelling the thermal coupling between internal power semiconductor dies of a water-cooled 3300V/1200A HiPak IGBT module", in *Proc. of the Conf. on Power Electronics, Intelligent Motion, and Power Quality (PCIM)*, Nuremberg, Germany, May 22 - 24, 2007.
- [3] H. Berg and E. Wolfgang, "Advanced IGBT modules for railway traction applications: reliability testing", *Microelectronics Reliability*, vol.38, no. 6, pp. 1319-1323, June 1998.
- [4] S. S. Manson, *Thermal stress and low cycle fatigue*, New York: McGraw-Hill, 1966
- [5] K. C. Norris and A. H. Landzberg, "Reliability of controlled collapse interconnections," *IBM Journal of Research and Development*, vol. 13, no. 3, pp. 266-271, May 1969.

- [6] R. Bayerer, T. Hermann, T. Licht, J. Lutz, and M. Feller, "Model for power cycling lifetime of IGBT modules – various factors influencing lifetime", in *Proc. of the 5<sup>th</sup> International Conference on Integrated Power Electronics Systems (CIPS)*, Nuremberg, Germany, March 11-13, 2008.
- [7] A. Hamidi, A. Stuck, N. Beck, and R. Zehringer, "Time dependent thermal fatigue of HV-IGBT-modules", in *Proc. of the 27<sup>th</sup> Kolloquium Halbleiter-Leistungsbaulemente und Materialgüte von Silizium*, Freiburg/Breisgau, Oct. 26 - 27, 1998.
- [8] M. P. Rodriguez, N. Y. A. Shamma, A. T. Plumptre, D. Newcombe, and D.E. Crees, "Static and dynamic finite element modelling of thermal fatigue effects in insulated gate bipolar transistor modules", *Microelectronics Reliability*, vol. 40, no. 3, pp. 455-463, March, 2000.
- [9] K. Sasaki, N. Iwasa, T. Kurosu, K. Saito, Y. Koike, Y. Kamita, and Y. Toyoda, "Thermal and structural simulation techniques for estimating fatigue of an IGBT module", in *Proc. of the 20<sup>th</sup> International Symposium on Power Semiconductor Devices and IC's (ISPSD)*, Orlando, Florida, USA, May 18-22, 2008.
- [10] W.W. Lee, L.T. Nguyen, and G.S. Selvaduray, "Solder joint fatigue models: review and applicability to chip scale packages", *Microelectronics Reliability*, vol. 40, no. 2, pp. 231-244, Feb. 2000.
- [11] M. Ciappa, F. Carhognani, P. Cow, and W. Fichtner, "Lifetime prediction and design of reliability tests for high-power devices in automotive applications", *IEEE Transactions on Device and Materials Reliability*, vol.3, no.4, pp. 191-196, Dec. 2003.
- [12] J.-P. Clech, "Review and analysis of lead-free solder material properties", Online available at: <http://www.metallurgy.nist.gov/solder/clech/Introduction.htm>
- [13] C. H. Raeder, L.E. Felton, R.W. Messler, and L.F. Coffine, "Thermomechanical stress-strain hysteresis of Sn-Bi eutectic solder alloy", in *Proc. of the IEEE/CPMT Int. Electronics Manufacturing Technology Symposium*, Las Vegas, May 21-14, 1995.
- [14] G. Z. Wang, Z.N. Cheng, K. Becker and J. Wilde, "Applying ANAND model to represent the viscoplastic deformation behaviour of solder alloys", *Journal of Electronic Packaging*, vol. 123, no. 3, pp. 247-254, Sept. 2001.
- [15] X.Q. Shi, Z. P. Wang, Q.J. Yang, and H.L.J. Pang, "Creep behaviour and deformation mechanism map of Sn-Pb eutectic solder alloy", *Journal of Engineering Materials and Technology*, vol. 125, pp. 81-87, Jan. 2003
- [16] N.E. Dowling, *Mechanical behaviour of materials: engineering methods for deformation, fracture, and fatigue*, Prentice-Hall, Inc., 1993.
- [17] U. Drogenik, I. Kovacevic, R. Schmidt, and J.W. Kolar, "Multi-domain simulation of transient junction temperatures and resulting stress-strain behaviour of power switches for long-term mission profile", in *Proc. of the 11<sup>th</sup> IEEE Workshop on Control and Modeling for Power Electronics (COMPEL)*, Zurich, Switzerland, Aug. 18-20, 2008.
- [18] A. Stupar, D. Bortis, U. Drogenik, and J. W. Kolar, "Advanced setup for thermal cycling of power modules following definable junction temperature profiles", in *Proc. of International Power Electronics Conference - ECCE Asia- (IPEC)*, Sapporo, Japan, Jun 21-24, 2010.